Deflection and Diffusion of a Rectangular Jet by the Edge Suction Effect

EDWARD S. TILLMAN JR.*
American Radiator and Standard Sanitary Corp., New Brunswick, N.J.

AND

FERNANDO SISTO JR.†
Stevens Institute of Technology, Hoboken, N.J.

The deflection of a two-dimensional, incompressible, irrotational jet by a suction slot located near the point of discharge has been analyzed both analytically and experimentally. Experiments show that the size, orientation, and suction flow rate of the slot have an influence on its effectiveness as a jet deflecting device. In order to explain this behavior from hydrodynamic principles, two mathematical models are proposed and solved. The first model simulates the case in which the slot is oriented in the plane of the upstream confining wall of the jet nozzle. The second model simulates the case in which the slot is so oriented that suction flow is into the perpendicular end face of the jet nozzle. In both models, the slot is simulated by a line sink and the boundaries of the jet by free streamlines. A conformal mapping technique is developed which carries the unit semicircle of an auxiliary plane onto the appropriate model in the physical plane, thus giving the streamline pattern, the jet deflection, and the downstream jet velocity. Experimental values for the jet deflection are presented which correlate well with those predicted by theory. Possible application of this principle in a fluid amplifier device is discussed.

Nomenclature

C = diffusion coefficient
d = half offset of jet
h = attachment length of flow around the corner
m = sink strength expressed as fraction of total jet flow
Q = magnitude of velocity vector in physical plane
s = suction slot opening
u = complex number in infinite half-plane (u plane), $u = x_1 + iy_1$
v = complex number in semicircle plane (v plane), $v = x + iy$
w = complex potential function, $w = \phi + i\psi$
W = distance between confining walls of jet
z = complex number in physical plane (z plane)
α = direction of velocity vector in physical plane
δ = deflection angle of freejet far downstream
ϕ = velocity potential function
ψ = stream function
Ω = function defined by $\Omega = -\log Qe^{-i\alpha}$

THE control of freejets has received considerable attention in recent years, particularly in the fields of rocketry and fluid amplifiers. Most presently used jet deflection systems employ injection of a secondary control flow to change the direction of the main jet flow. The deflection technique discussed in this paper, however, employs suction applied through a narrow slot at the jet exit to control the jet direction. This phenomenon was discovered and first documented by Heskestad[1] and is termed the "edge suction effect."

A schematic drawing showing the location and orientation of the suction slot is presented in Fig. 1. Early exploratory work performed by Heskestad and later confirmed by Tillman[2] showed that, in addition to the suction rate, both the size and orientation of the suction slot had an influence on its effectiveness as a jet deflecting device. For example, it was found that when the slot was oriented in the plane of the upstream confining wall (0° orientation), the jet deflection angle decreased with increasing slot size for one fixed suction rate. However, when the slot was oriented so that suction flow was into the perpendicular end face of the confining wall (90° orientation), the opposite effect occurred and the deflection increased with increasing slot size for a fixed suction rate (at least in certain suction flow ranges). Of course, when a real fluid flows through the jet, the suction slot removes flow from the wall boundary layer, and this removal has some effect on the freejet structure. In order to rationalize the behavior of the suction slot with respect to size and orientation, and to determine how much of a contribution the boundary-layer removal has on the jet deflection, an analytical study was undertaken of an idealized jet. The

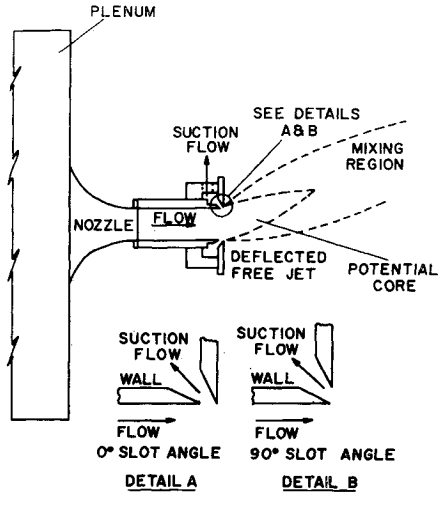

Fig. 1 Simplified sketch of jet showing details of slot orientation.

Received November 28, 1966. [3.01]

* Supervisor, Heat Transfer Research, Research Division; now Associate Professor of Mechanical Engineering, University of of Bridgeport, Bridgeport, Conn.

† Professor of Mechanical Engineering and Head of the Department. Associate Fellow AIAA.

results of both the analytical study and an experimental investigation of this phenomenon are discussed in this paper.

Actually, two mathematical models were proposed: one representing the 0° slot orientation (Model I), and the other representing the 90° slot orientation (Model II). These models are shown in Figs. 2 and 3 with the experimental jet structure superimposed. In these mathematical models, the suction slot is simulated by a line sink located in the plane of the wall at a distance from the end of the wall that corresponds to a point between the two edges of the physical slot. The confining walls of the stream are represented by straight streamlines, and the boundaries of the jet are represented by free streamlines, i.e., streamlines along which the magnitude of the velocity vector is constant. The flow is assumed to be incompressible, irrotational, and two-dimensional. These assumptions made it possible to develop a conformal mapping technique which yielded theoretically developed flowfields for various jet-sink combinations, and thus helped to explain some of the peculiarities of this phenomenon from basic principles.

Analytical Study of Model I

The freejet shown in Fig. 2 represents a more complicated case of the classic Helmholtz type problem discussed in most standard texts on fluid dynamics. In problems of this sort, neither the shape of the jet nor the magnitude of the downstream velocity are known. The model shown in Fig. 2 represents a further complication, in that the presence of a sink makes using Kirchhoff's method impractical. The method employed in this study is attributed to Hopkinson.[3] It consists of developing an analytic function that will map the unit semicircle shown in Fig. 4 onto the z plane of Fig. 2, thus giving the free streamline shape, the downstream velocity, and the jet deflection angle.

The development of the mapping function is covered in detail in Ref. 2 and is only outlined in this paper. The method employed consisted of developing two functions, $dw/dv = f_1(v)$ and $dz/dw = f_2(v)$. These functions were then combined and integrated to give $z = f(v)$, the required mapping function. The function $f_1(v)$ was developed from the complex velocity-potential function w for source and sink flow in the v plane. Although this function could have been developed directly in the v plane, a simpler approach was used. The velocity potential was first developed in an auxiliary u plane, the upper semi-infinite half plane shown in Fig. 4, and then transformed to the v plane by the inverse Joukowski function,

$$u = 2v/(1 + v^2) \tag{1}$$

The function $f_2(v)$ was developed from considerations, outlined by Hopkinson, of the behavior of the logarithmic hodograph function, $\Omega = -\log Qe^{-i\alpha}$, at points of velocity discontinuity and at infinity in the u plane. The resulting function was then transformed to the v plane by Eq. (1).

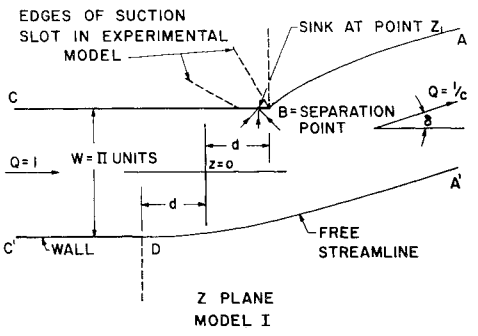

Fig. 2 Sketch of mathematical model of a freejet with a suction slot oriented at 0°.

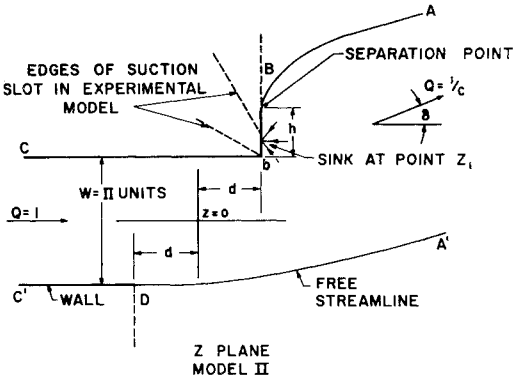

Fig. 3 Sketch of mathematical model of a freejet with a suction slot oriented at 90°.

The final result was obtained by combining $f_1(v)$ and $f_2(v)$ to eliminate $w(v)$ and integrated to give the required function,

$$z_0 = K_0 + HC_0[(F/2)\log(1 + v^2) + G \arctan v + C_1 \log(v - v_0) + D_1 \log(1 - v_0 v) + [E_1 v_1/(1 - v_1 v)] + E_2 \log(1 - v_1 v)] \tag{2}$$

The algebraic expressions for each of the constants are given in Table 1. This function transforms points on the semicircular arcs BA and DA' of the v plane to the free streamlines of the physical (z) plane, and interior streamlines in the v plane become the actual streamlines in the jet. The sink m at point v_1 maps to the point z_1 in the physical plane and the points CC' and AA' become, respectively, points far upstream and far downstream in the jet. From the requirements that the velocity be unity at the point CC' in the physical plane and that the point $v = +i$ becomes the point far downstream in the physical plane, two expressions were developed for the jet deflection and the diffusion coefficient,

$$\delta_0 = \arctan \frac{2(v_1 v_1' + 1)(v_1 - v_1')}{(v_1 v_1' + 1)^2 - (v_1 - v_1')^2} \tag{3}$$

$$C_0 = (1 - v_1 v_0)(v_0 - v_1')/(v_0 - v_1)(1 - v_1' v_0) \tag{4}$$

where v_1' is related to v_1, v_0, and m by

$$[v_1'/(1 + v_1'^2)](1 - m) = [v_1/(1 + v_1^2)] - [mv_0/(1 + v_0^2)] \tag{5}$$

Finally, expressions for the constant K and the half offset d were developed from the requirements that the point $v = -1$ maps onto $z = +d + (i\pi/2)$ and $v = +1$ maps onto $z = -d - (i\pi/2)$. These expressions are given as follows:

$$K_0 = -\frac{HC_0}{2}\left[F \log 2 + (C_1 + D_1)\log(1 - v_0^2) + \frac{2E_1 v_1}{(1 - v_1^2)} + E_2 \log(1 - v_1^2)\right] - \frac{i\pi}{2} \tag{6}$$

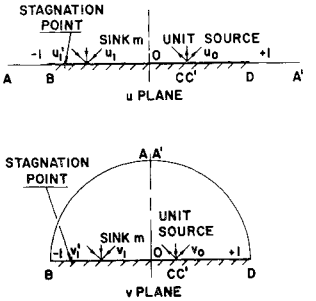

Fig. 4 Auxiliary u and v planes for the model shown in Fig. 2.

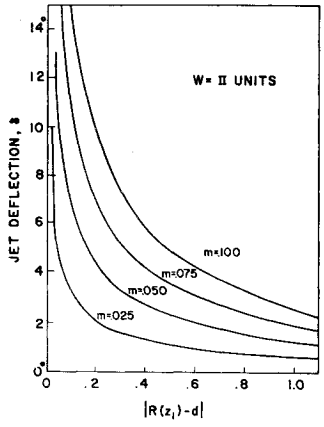

Fig. 5 Analytically determined values of jet deflection plotted as a function of sink location for various sink strengths, 0° slot orientation and $-0.002 < d < +0.002$.

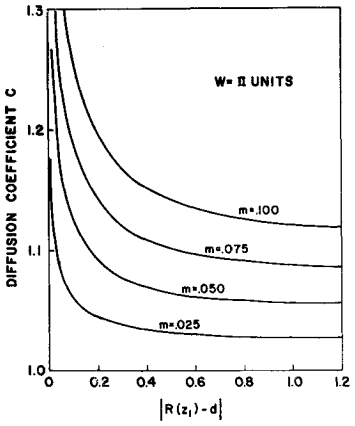

Fig. 6 Analytically determined values of the diffusion coefficient plotted as a function of sink location for various sink strengths, 0° slot orientation and $-0.002 < d < +0.002$.

$$d_0 = \frac{HC_0}{2}\left[-\frac{\pi}{2}G + (C_1 + D_1)\log\left(\frac{v_0+1}{1-v_0}\right) - \frac{2E_1v_1^2}{(1-v_1^2)} - E_2\log\left(\frac{1-v_1}{1+v_1}\right)\right] \quad (7)$$

Equations (3, 4, and 7) express the important jet characteristics δ, C_0, and d_0 in terms of the parameters v_1, v_0, and m. Thus, for each choice of these three parameters a particular jet structure is determined. The sink location z_1, corresponding to the choice of parameters, can be determined by substituting $v = v_1$ into Eq. (2) and, together with the expression for K [Eq. (6)] solving for z_1. Similarly, the stagnation-point location z_1' can be determined by solving Eq. (5) for v_1' and substituting this value, $v = v_1'$, into Eq. (2). The main problem with this technique is that the location of the sink of strength m in the v plane is of no physical significance. Usually, one is interested in the jet structure produced by a sink of known strength, located at a specific point z_1 and a specified offset $2d$. (For this study, only jets with zero offset were studied.) Equations (2–7) were programmed for computer solution and solved for several different values of m. The parameters v_1 and v_0 were varied over a range of values and the computed results were plotted. These families of curves were then cross-plotted to determine values of δ_0, C_0, and z_1 at those combinations of v_1, v_0, and m which made $d = 0$. Typical results are presented in Figs. 5 and 6. As can be seen from these curves, the effectiveness of the sink as a jet deflecting and diffusing device becomes much stronger as it approaches the end of the solid confining wall. In fact, in the limit, regardless of sink strength, δ approaches 90° and C becomes large.

Table 1 Definition of constants used in equations

$$C_1 = \frac{-v_0v_1^2(1-v_1'v_0)^2}{(1-v_1v_0)^2(1+v_0^2)}$$

$$D_1 = \frac{-v_0v_1^2(v_0-v_1')^2}{(v_1-v_0)^2(v_0^2+1)}$$

$$E_1 = \frac{v_0(v_1^2-1)(v_1-v_1')^2}{(v_1^2+1)(1-v_0v_1)(v_0-v_1)}$$

$$E_2 = v_1\frac{\left\{\begin{array}{l}(v_1^2+1)(1-v_0v_1)[(v_0-v_1)/v_0]\times \\ \qquad [2(v_1^2-1)(v_1'^2-v_1v_1')-2(v_1-v_1')^2]- \\ (v_1^2-1)(v_1-v_1')^2\{4(v_1^2+1)- \\ \qquad v_1(3+v_1^2)[v_0+(1/v_0)]\}\end{array}\right\}}{(v_1^2+1)^2(1-v_0v_1)^2[(v_0-v_1)/v_0]^2}$$

$$E_b = \frac{-\left[\frac{E_1(1-v_1v_b)(v_1^2l+2v_1)}{2(v_1^2+lv_1+1)} - E_1v_1 - E_2(1-v_1v_b)\right]}{(-(v_1^2+lv_1+1))^{1/2}}$$

$$F = \frac{2v_0v_1^2}{(v_0^2+1)(v_1^2+1)^2}[(1+v_1v_1')^2-(v_1'-v_1)^2]$$

$$G = \frac{4v_0v_1^2}{(v_0^2+1)(v_1^2+1)^2}[(v_1'-v_1)(1+v_1'v_1)]$$

$$H = \frac{-(1-m)(1+v_0^2)(1+v_1^2)}{(1+v_1'^2)v_0v_1^2}$$

$$C_0 = \frac{(1-v_1v_0)(v_0-v_1')}{(v_0-v_1)(1-v_1'v_0)} \qquad l = \frac{1+v_b^2}{-v_b}$$

$$L = (X+Y)/(2l)^{1/2} \qquad N = (X-Y)/(2l)^{1/2}$$

$$X = \frac{v_0v_1^2}{(v_0^2+1)(v_1^2+1)^2}\times [2(v_1'-v_1)(1+v_1v_1') - v_b[(1+v_1v_1')^2-(v_1'-v_1)^2]]$$

$$Y = \frac{v_0v_1^2}{(v_0^2+1)(v_1^2+1)^2}\times [(1+v_1v_1')^2-(v_1'-v_1)^2+2v_b(v_1'-v_1)(1+v_1v_1')]$$

Experimental Verification of the Analytical Solutions for Model I

A brief experimental investigation was conducted to measure the magnitude of the effect and to verify the analytically predicted jet deflection angles. A schematic drawing of the apparatus is shown in Fig. 7. The total flow through the jet and the suction flow were measured by orifice meters. Provision was made for boundary-layer removal upstream of the suction slot through a porous section of the jet confining wall. The jet nozzle consisted of a converging section and a 7½-in.-long rectangular duct 10 in. wide by 2½ in. high. This nozzle was modified so that experiments could also be made on a 1-in.-high jet. Screens and baffles were

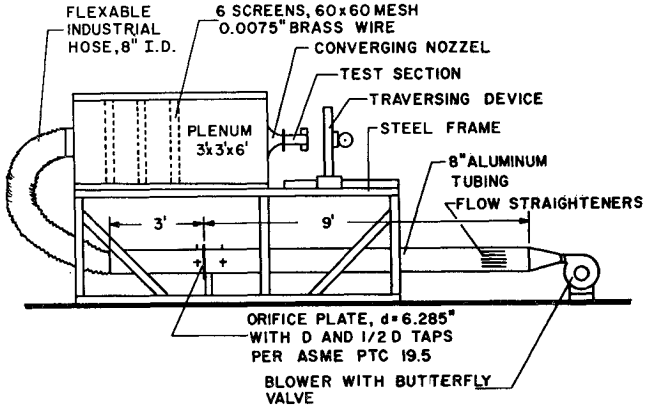

Fig. 7 Schematic drawing of experimental apparatus showing major components.

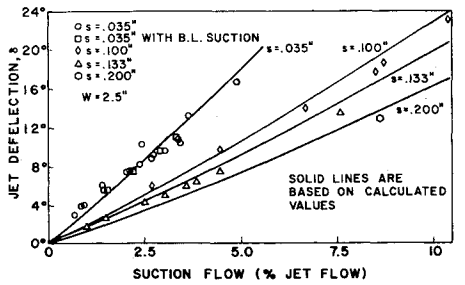

Fig. 8 Experimental and theoretical values of jet deflection for various suction rates and slot sizes, 0° slot orientation.

placed in the plenum to insure uniform, low-turbulence flow upstream. The jet deflection angles and the downstream velocity in the potential core of the jet were measured by a 3-hole, angle-measuring probe and a vernier protractor. This probe was held in a suitable traversing device and was connected to precision manometers. The zero reference angle was obtained for the undisturbed jet by centering the probe in the freejet, one jet height downstream from the exit plane. The probe was rotated until a zero pressure gradient was measured across the two angle-measuring taps. This angular orientation represented the zero reference of the jet. The deflection angle of the jet obtained while suction was applied was determined by traversing the deflected jet at a point one jet height downstream to determine the center of the potential core. The rotation of the probe from the zero reference angle which again gave a zero pressure differential, was then recorded at this center point and was called the jet deflection angle. The velocity of the potential core was measured by means of the total pressure tap in the probe. This velocity was compared to the measured velocity in the exit plane of the jet obtained, when the same quantity of air flowed through the jet, but without suction. The ratio of these two measured velocities gave the diffusion coefficient C.

The results of the measured jet deflection angles as functions of suction rate are presented in Fig. 8 for several different slot openings. These are compared to theoretical curves derived from the curves shown in Fig. 5. As can be seen from Fig. 5, the effectiveness of the sink as it approaches the end of the jet wall becomes very sensitive to its position. Therefore, it is important to choose a representative sink location accurately, in order to develop the correct theoretical curve. It was assumed that the flow patterns into the slot would be similar, regardless of the size of the slot opening or suction rate, so that the relative position of the sink in the slot, which would most closely simulate the actual flowfield into the slot, would remain unchanged. Several sink locations, expressed as a fraction of the slot width from the end, were used to develop different families of theoretical curves. The sink position which best fitted the experimental data was located at a distance $\frac{1}{3}$ of a slot width from the end of the jet. This position corresponds, qualitatively, to the position one would expect in the slot. Figure 9 shows a photograph of the suction flow traced by dye in a water model of the slot. Note that the flow is concentrated near the vicinity of the end of the jet.

The experimentally determined fact that the deflection angle decreases for a given suction rate as the slot opening increases, is also verified by the theoretical curves. Opening the slot in the experimental model is equivalent to moving the sink upstream in the theoretical model. As demonstrated by the solutions shown in Fig. 5, the sink has less effect on the jet when it is moved upstream.

Values of the diffusion coefficient were obtained and are presented in Fig. 10. From this figure it can be seen that the measured values of the diffusion coefficient do not correspond well to the theoretical curves. In fact, experimental

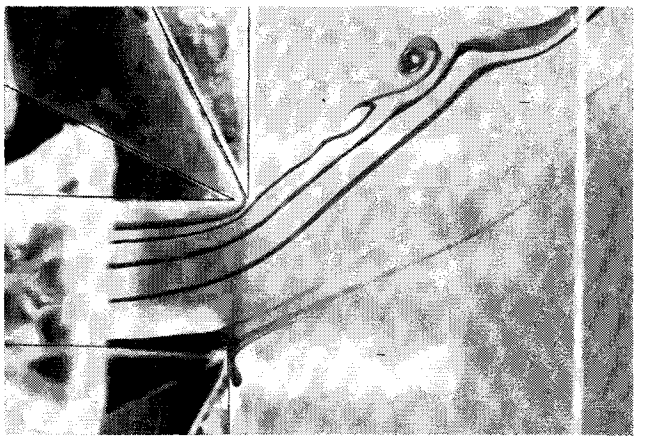

Fig. 9 Photograph of water model of two-dimensional freejet. The flow was traced by dye injected upstream at the left. The suction flow rate was 24% of the main jet flow and the slot opening was 10% of the jet height which was 1 in. To compensate for focusing and parallax errors, the actual edges of the walls of the jet have been outlined by ink in this photograph.

points only follow the general trend of the theoretical curves. This poor agreement is due, in part, to the fact that flow separation occurred on the side walls of the jet when suction was applied. This is not too surprising because streamline plots, developed from the theoretical analysis discussed in the previous section, showed that in the vicinity of the slot the velocity decreases rapidly with a subsequent pressure rise. This adverse pressure gradient caused boundary-layer separation on the side walls and the separated jet behaved in a three-dimensional manner, with the velocity component directed toward the center plane from the side walls. Since C was developed from the two-dimensional continuity equation, the poor agreement with the experimental values can be expected. A second contributing factor to the poor agreement between the experimental and theoretical values of the diffusion coefficient may be due to the approximation of the turbulent-mixing regions by free streamlines. This turbulent mixing occurs more or less equally on the upper and lower free boundaries of the jet. The result is a reduction in the width of the potential core of the jet, which counteracts the tendency of the jet to spread and to decelerate. Since this erosion of the potential core occurs symmetrically with respect to the central streamline, the effect on the experimental value of C is much greater than the effect on the experimental value of the jet deflection.

Analytical Study of Model II

The case of the 90° slot orientation was solved analytically in the same manner as the 0° slot using the model shown in Fig. 3. This case was complicated by the inclusion of the

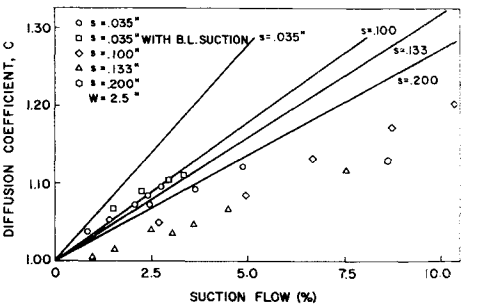

Fig. 10 Experimental and theoretical values of the diffusion coefficient for various suction rates and slot sizes, 0° slot orientation.

right-angle break in the confining wall and by the separation length. Early exploratory experiments, using smoke and oil films for flow visualization, had shown that for the 90° slot orientation, separation did not always occur at the tip of the suction slot. Instead, the jet flow remained attached to the end wall some short distance before separation occurred. This distance was found to be of the order of a few slot widths for the conditions investigated.

A development similar to that presented earlier was followed. The function $f_1(v)$ was identical to the one developed for the 0° slot orientation since the arrangement of sources and sinks in the v plane is identical for the two cases. The function $f_2(v)$ was modified, however, to include the effect of the infinite velocity at the corner b in the physical plane. Combining and integrating these two functions gave a new function that mapped the semicircular v plane onto the physical plane shown in Fig. 3. This function is given as follows:

$$z_{90} = K_{90} + g(v)$$

$$z_{90} = K_{90} + \frac{H}{(-v_b)^{1/2}} C_{90}\Bigg\{(L - iN)\log[P(v) + iQ(v)] + (L + iN)\log[P(v) - iQ(v)] + \frac{C_1(v_0 - v_b)}{(v_0^2 + lv_0 + 1)^{1/2}} \times \log\left[\frac{2(1 + v_0v) + l(v + v_0) - 2[(v_0^2 + lv_0 + 1)(v^2 + lv + 1)]^{1/2}}{v - v_0}\right] + \frac{D_1(v_0v_b - 1)}{(v_0^2 + lv_0 + 1)^{1/2}} \times \log\left[\frac{lv_0(1 + v_0v) + 2v_0(v_0 + v) + 2v_0[(v_0^2 + lv_0 + 1)(v^2 + lv + 1)]^{1/2}}{1 - v_0v}\right] + \frac{E_1v_1^2(1 - v_bv_1)}{(v_1^2 + lv_1 + 1)} \frac{(v^2 + lv + 1)^{1/2}}{1 - v_1v} + E_b \log\left[\frac{lv_1(1 + v_1v) + 2v_1(v_1 + v) + 2v_1i[-(v_1^2 + lv_1 + 1)(v^2 + lv + 1)]^{1/2}}{1 - v_1v}\right]\Bigg\} \quad (8)$$

where

$$P(v) = \frac{l(v^2 - 1) + (1 - v)[2l(v^2 + lv + 1)]^{1/2}}{v^2 + 1} \qquad Q(v) = \frac{2(v^2 + lv + 1) - (1 + v)[2l(v^2 + lv + 1)]^{1/2}}{v^2 + 1}$$

The constants are defined in Table 1 in terms of v_1, v_0, v_b, and m.

In addition to the parameters v_1, v_0, and m, this function contains the added parameter v_b; i.e., the location of the point in the v plane which corresponds to the corner in the z plane (physical plane). By introducing the condition that the velocity must be unity at the point CC' in the physical plane and that the point $v = +i$ becomes the point far downstream in the physical plane, two new expressions were developed for the jet deflection angle and diffusion coefficient.

$$\delta_{90} = \arctan\left\{\frac{[-(v_1 - v_1')^2 + (1 + v_1v_1')^2][\frac{1}{2} - (1/l)]^{1/2} + 2(v_1 - v_1')(1 + v_1v_1')[\frac{1}{2} + (1/l)]^{1/2}}{[-(v_1 - v_1')^2 + (1 + v_1v_1')^2][\frac{1}{2} + (1/l)]^{1/2} - 2(v_1 - v_1')(1 + v_1v_1')[\frac{1}{2} - (1/l)]^{1/2}}\right\} \quad (9)$$

$$C_{90} = \frac{(1 - v_1v_0)(v_0 - v_1')}{(v_0 - v_1)(1 - v_1'v_0)}\left(\frac{(1 - v_bv_0)}{(v_0 - v_b)}\right)^{1/2} = C_0\left(\frac{1 - v_bv_0}{v_0 - v_b}\right)^{1/2} \quad (10)$$

Next, the transform conditions given below were introduced into Eq. (8)

$$\left.\begin{array}{ll} \text{when } v = -1 & z_{90} = d + [h + (\pi/2)]i \\ \text{when } v = +1 & z_{90} = -d - (\pi/2)i \\ \text{when } v = v_b & z_{90} = +d + (\pi/2)i \end{array}\right\} \quad (11)$$

This yielded the following expressions for K_{90}, d_{90}, and h in terms of v_0, v_1, v_b, and m:

$$K_{90} = -\tfrac{1}{2}[g(+1) + g(v_b)] \quad (12)$$

$$d_{90} = -(i\pi/2) + \tfrac{1}{2}[g(v_b) - g(+1)] \quad (13)$$

$$h = \text{Imag Part}\{K_{90} + g(-1)\} - (\pi/2) \quad (14)$$

These involved algebraic expressions were programmed for solution on a digital computer. For each choice of the parameters v_1, v_0, v_b, and m, the values for the sink location, the stagnation point location, d_{90}, h, δ_{90}, and C_{90} were obtained. Since experiments were only performed on jets with zero offset, the program was modified to give solutions for combinations of the parameters which gave values of $d_{90} = 0$. This was done by making v_1, v_b, and m the independent variables, and for each choice of these variables, an iterative technique was programmed which found the corresponding value of v_0 that made $d = 0$.

The problem of choosing those combinations of parameters which correspond to physically realized situations deserves some comment. No simple presentation of the deflection vs sink location can be made because of the presence of the separation length. It was shown that, for a particular sink strength, the sink location and the separation length had an influence on the jet structure. Any correlation between these theoretical solutions and experimental data requires an accurate determination of the separation length, as well as an effective sink location.

Experimental Verification of the Analytical Solutions for Model II

Experiments were performed on the jet with a 90° slot orientation using the apparatus described earlier in this paper. The separation length was measured by two techniques. The first method consisted of covering the vertical end wall of the jet with a film of colored oil. When edge suction flow was started, this oil film was pushed a short distance away from the slot and this distance was measured with a machinist ruler. The second method consisted of injecting smoke into the turbulent boundary of the jet and observing and measuring the point of separation. In most cases, this method gave slightly larger separation lengths than the oil film technique. It was assumed that the oil film was subjected to surface tension and gravity forces which gave erroneous readings. In most cases, over the range of slot sizes and suction rates investigated, the separation length was of the order of a few slot openings.

A second experimental fact was noted which was used to establish the correct analytical parameters. This was the location of the stagnation point. Smoke and oil film tests had shown that for edge suction flow conditions the stagnation point always resided at the tip of the suction slot. Thus, rather than fix a sink location, a stagnation-point location was chosen in the physical plane which corresponded to the tip of the suction slot in the experimental model. In the

Table 2 Comparison of experimental and theoretical values of C, the diffusion coefficient, 90° slot orientation

s, in.	% Suction	Jet velocity, no suction, ft/min	C experimental	C theoretical
0.015	2.1	3390	1.22	1.417
0.015	2.8	3390	1.22	1.428
0.015	3.5	3390	1.23	1.440
0.015	4.2	3390	1.24	1.450
0.015	2.3	2020	1.12	1.421
0.015	3.9	2020	1.15	1.446
0.015	5.3	2020	1.17	1.468
0.015	6.4	2020	1.17	1.485
0.015	7.5	2020	1.19	1.502
0.030	4.2	3390	1.26	1.527
0.030	6.3	3390	1.27	1.552
0.030	7.1	3390	1.23	1.561
0.030	4.2	3500	1.28	1.527
0.030	6.3	3500	1.30	1.552
0.030	7.3	3500	1.32	1.563
0.030	4.2	3410	1.27	1.527
0.030	5.4	3410	1.28	1.541
0.030	6.2	3410	1.29	1.550
0.030	7.3	3410	1.30	1.563
0.050	5.4	3320	1.27	1.599

theoretical solutions for the jet with $d = 0$, one can pick values for the parameters v_1, v_b, and m such that a particular sink location and separation length is obtained. The stagnation-point location can then be determined since it is related to the locations of z_1 and h in the physical plane. Conversely, a combination of the parameters v_1, v_b, and m can be chosen which gives a desired stagnation-point location and separation length. The corresponding sink location can then be determined. Theoretical curves were developed by this method for slot sizes of 1.5, 3.0, and 5.0% of the jet height. These are shown in Fig. 11. Corresponding experimental points are shown on the same figure. Although the theoretical curves are shown for a range of suction flows from 0 to 12.5%, true edge suction flow conditions exist over a narrower range. At very low suction rates, edge suction flow is not established and the suction slot draws most of its flow from the quiescent ambient air. At high suction rates, where the jet experiences large deflections of the order of 60°, the Coanda effect seems to take over and the jet attaches to the end wall and experiences a deflection of 90° for all suction rates above this critical value.

Several experimental values for the diffusion coefficient are compared to theoretical values in Table 2. These experimental values for the diffusion coefficient did not agree well with those predicted by theory. The same reasons that were proposed for the poor agreement for the case of the 0° slot orientation also hold for this case. The problem of non-two-dimensional flow was even more severe for this case because, in general, greater deflection angles and greater velocity changes were experienced.

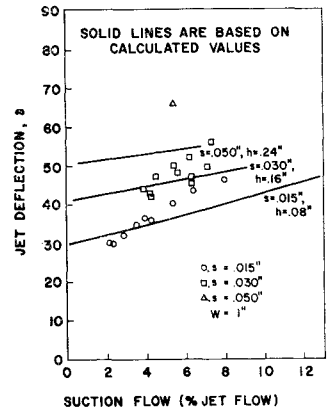

Fig. 11 Experimental and theoretical values of jet deflection for various suction rates and slot sizes, 90° slot orientation. Only data for fully established "edge suction effect" conditions are shown.

Conclusions and Significance of the Results

The two analytical models shown in this paper are idealized representations of the freejet with a suction slot oriented at the two extremes of 0° and 90°. The theoretically calculated jet deflection angles correspond well to those obtained experimentally and confirm the influence of the suction slots on the jet behavior. In addition, since the solutions were developed for pure potential flow without the inclusion of boundary-layer considerations and these solutions appear to correspond well to experimental data, the conclusion was made that boundary-layer removal by the suction slot has only a secondary influence on the jet behavior. Because of the apparent reliability of the theoretical solutions, these models could be used to predict the behavior of other combinations of suction rate and slot openings.

The purpose of the work presented in this paper was to develop an understanding of the behavior of the suction slot on the freejet. However, two important practical result should be emphasized since they might be applicable to fluid amplifier design. The first of these can be seen by referring to Fig. 8. For the case of the 0° slot orientation it can be seen that the deflection is almost a linear function of the suction rate. This fact was confirmed by experiments. This feature suggests that the 0° slot orientation might be used in a proportional fluid amplifier device. The second feature can be seen from Fig. 11. Here, small suction flows of the order of 2% of the main jet flow will produce a deflection of as much as 30°. This suggests that the 90° slot orientation might be used in a flip-flop type amplifier with a high flow gain.

References

[1] Heskestad, G., "An edge suction effect," AIAA J. **3**, 1958–1961 (1965).

[2] Tillman, E. S., "Deflection and diffusion of a two-dimensional free jet by suction," ScD thesis, Stevens Institute of Technology (1965).

[3] Hopkinson, B., "On discontinuous fluid motions involving sources and vortices," Proc. London Math. Soc. **29**, 142–164 (1898).